# CONTROLLER DESIGN AND ANALYSIS OF UNMANNED AERIAL VEHICLES USING AUTOMATIC GAIN GENERATION TECHNIQUE

**Dong-Wan Yoo* and Min-Jea Tahk****
***KAIST, ****KAIST**
*dwyoo@fdcl.kaist.ac.kr; mjtahk@fdcl.kaist.ac.kr*

## Abstract

*This paper deals with the controller design and analysis of Unmanned Aerial Vehicles (UAVs), which are highly developed and widely spread out throughout the entire world. The importance of UAVs grows every year in various missions, and these UAVs are required to show their best performances. In order to have a good performance for an UAV, a proper controller design technique should be considered along with its proper analysis. In this paper, a controller design procedure eligible for various types of UAVs is introduced and applied to an UAV model. Also, this paper presents an automatic gain generation technique, which is a useful tool for a designer who desires to generate the gains of the UAV autopilot system automatically, which is followed by a linear analysis of the controller for the verification.*

## 1 Introduction

The needs for unmanned aerial vehicles (UAVs) are growing exponentially over the years. Their applications could be easily found in many areas such as rescue, military surveillance and reconnaissance, civilian missions, etc [1]. As the UAVs are assigned to more important and more extensive missions these days, they are greatly obligated for the accomplishments in those missions. Such accomplishments come from successful designs of the controllers that are implemented on the UAVs. Therefore, it is very essential to design a controller with a proper design procedure and to perform an adequate controller analysis followed by numerous simulation studies.

In many practical UAV designs, the most widely used controller is Proportional Integral Derivative (PID) controller. PID controller requires a precise control gain design from each part of the controller to give the accurate commands to the control surfaces. Usually, this process is carried out by hands of engineer's intuitions and numerous trials and errors. In order to have satisfied responses from each channel, a user should apply a reasonable gain values to each control channel. However, since the user should apply different gains for different models, finding the gains for each controller by hands will not be delightful in time-wise. Hence, there must be an automation process in the design procedure. The automatic gain generation technique extracts automated gains rather than hand made gains. With the only parameters a designer has to decide, which are damping and pole location of each control parts, the designer is able to obtain the optimal gain set for the given UAV model.

This paper starts with UAV trim and linearization, followed by stability augmentation system (SAS) and control augmentation system (CAS) designs, autopilot design, and finally, linear analysis, which is a verification process to check the designed controllers from previous sections. Several nonlinear simulations are conducted as the final assessments of the whole process of designing.

## 2 Trim and Linearization Algorithms

Trim and linearization processes enable the user to perform simpler linear analyses on the designed aircraft model. Following algorithms explain trim and linearization processes.

## 2.1 Trim Algorithm

Trim algorithm is used to obtain the values for the state variables and the control variables of an aircraft when the aircraft is in an equilibrium state. Usually, there are three types of equilibrium states that can be applied to an aircraft [2,3]. The most widely calculated equilibrium state is the level flight. In this case, sum of total forces and moments are zero, and the aircraft maintains its altitude with a constant airspeed. For the level flight trim condition, there are three assumptions applied for the flight condition: straight, symmetrical and level flight. From the assumptions, the following condition can be applied.

$$\delta_a, \delta_r, \beta, p, q, r, Y, L, M = 0 \qquad (1)$$

Where $\delta_a, \delta_r, \beta, p, q, r, Y, L, M$ are aileron deflection, rudder deflection, sideslip angle, roll, pitch, and yaw rates, side force, roll and yaw moments, respectively. By cancelling all the terms in equation (1), a vector with forces and moments and a control input vector are simplified as equation (2), which shows the forces and moments in the longitudinal direction, and control inputs to be applied to hold the aircraft at a trimmed state.

$$\phi = [X \quad Z \quad M]^T, \quad x = [\alpha \quad \delta_e \quad \delta_T]^T \qquad (2)$$

where $X$, $Z$ are the forces in x and z directions, $M$ is the pitching moment, $\alpha$ is angle of attack, $\delta_e$ is elevation deflection in degrees and $\delta_T$ is the throttle level in percentages.

The purpose is to find the control input values, which make the system with zero forces and moments by using modified Newton-Raphson method, expressed in equation (3).

$$\phi(x + \delta x) = 0 \approx \phi(x) + \frac{\partial \phi}{\partial x}\delta x \qquad (3a)$$

$$\delta x = -\left[\frac{\partial \phi}{\partial x}\right]^{-1} \phi(x) \qquad (3b)$$

As it is shown in equation (3), the algorithm suggests that the perturbation parameter $\delta x$ is to be added to the original state, and the result can be derived as the right side of equation (3a). $\partial\phi / \partial x$ is the Jacobian matrix of $\phi$. As perturbation approaches to some tolerance value near zero, the algorithm terminates and outputs the trim condition values ($\delta_{e_{trim}}, \delta_{T_{trim}}, \alpha_{trim}$).

## 2.2 Linearization Algorithm

Once the trim process is finished with the output trimmed values, linearization process is to begin. Linearization is the process which derives a linear model from a nonlinear model of an aircraft. Linearization of an aircraft defines the aircraft motion as the trimmed state motion plus a disturbance motion. Equation (4) expresses such statement.

$$x = x_e + \Delta x \qquad (4)$$

$$f(x) = f(x_e + \Delta x) \approx f(x_e) + \left(\frac{\partial f}{\partial x}\right)_{x_e} \Delta x \qquad (5)$$

$$\Delta \dot{x} = \left(\frac{\partial f}{\partial x}\right)_{x_e} \Delta x \equiv A \Delta x \qquad (6)$$

In equations (4), $x_e$ and $\Delta x$ are equilibrium state and disturbance, and equation (5) is the representation of 1st order Taylor Series Expansion of equation (4). However, since trim condition $f(x_e)$ is zero from the trim algorithm, final expression for the linearization is in equation (6). Jacobian matrix $(\partial f / \partial x)_{x_e}$ in equation (6) corresponds to $A$ (or $B$) matrix, which is the linearized model of the aircraft. Detailed expressions for A and B matrices in longitudinal and lateral sections can be found in [2].

## 3 SCAS and Autopilot Design

In this section, SCAS design structures and autopilot systems for longitudinal and lateral channel are separately described. References for this section and the next section are [2-6].

### 3.1 Longitudinal SCAS and Autopilot

Longitudinal SCAS and autopilot structures are represented in figure 1.

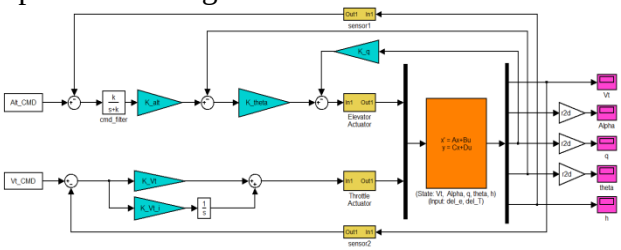


Fig. 1. Longitudinal SCAS and autopilot

As it is shown in figure 1, the longitudinal control loop is composed of a pitch loop, an altitude loop, and a velocity loop. Pitch ($\theta$) loop is the most inner control structure surrounding the pitch rate ($q$) loop, which behaves as a damper in the pitch loop. As the figure suggests, the control commands for the longitudinal autopilot system are altitude and total velocity of the aircraft. Autopilot structure in figure 1 suggests that the altitude is controlled by the changes in pitch angle led by aircraft's elevator deflection angle. Total velocity ($V_T$) of the aircraft is controlled by the velocity loop structure, which is controlled solely by the thrust level of the engine. An alternate type of the controller called 'throttle based altitude control (TBAC)' structure is introduced along with the conventional type. As its name suggests, an aircraft, which is designed with TBAC structure, controls its altitude with the thrust level of the engine and controls its total velocity by the pitch angle [6]. TBAC control structure is displayed in figure 2.

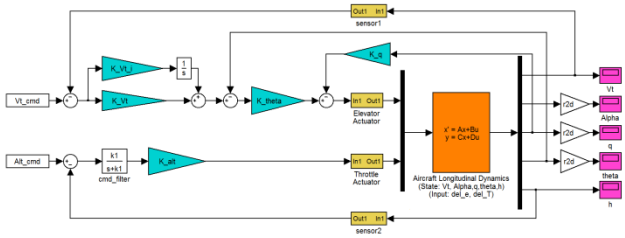


Fig. 2. TBAC Control Structure

One may notice that the pitch SCAS loop inside the altitude loop of conventional type structure is similar to the one inside the velocity loop of the TBAC. Reasons for designing the SCAS and autopilot in this way are as follows. First, by controlling the altitude with the throttle, passengers in the aircraft would feel less inclination or declination in the cabin for the case of takeoff and landing, so that this method is used mostly in commercial airliners. Also, for the case of the engine failure, the velocity of the aircraft can be adequately controlled by the elevator, which enables the gliding function of the aircraft. With numerous advantages it contains, the TBAC structure is also applied for several UAVs as well; one good example is RQ-101 Night Intruder 300 (Korea Aerospace Industries). For a precise control of the velocity and altitude, the system must be carefully designed with the consideration of the coupling effects from both altitude and velocity control channels. As the aircraft tries to gain the altitude by increasing thrust level, the velocity tends to decrease since there is no aid from the thrust channel to compensate for the velocity loss and vice versa. Similar phenomenon occurs when the aircraft gains the speed; the aircraft has to give up its altitude and vise versa. Therefore, there must be a proper sequential logic applied to the control structure with adequate gain selections, which will be the main topic of section 4.

## 3.2 Lateral SCAS and Autopilot

Lateral SCAS includes roll rate ($p$) loop and yaw rate ($r$) loop with proper gain values and washout filters. Since the functions of those rate loops are to improve the dampings of corresponding channels, those loops are called roll damper and yaw damper, respectively. Also, the outer loop of the roll rate loop is roll angle loop ($\phi$), which decides the bank angle of the plane. Application for the Aileron-Rudder Interconnection (ARI) sytstem is also required to compensate for the adverse yaw problem. Lateral SCAS and autopilot is depicted in figure 3.

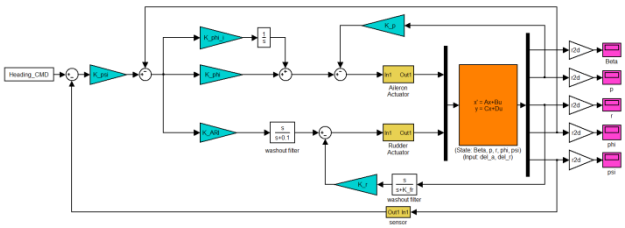


Fig. 3. Lateral SCAS and autopilot

Lateral autopilot system is also referred as heading hold autopilot system. Heading hold autopilot system keeps the roll angle control system as its inner loop system. Control command for the whole lateral autopilot system is the heading angle of the aircraft.

## 4 Automatic Gain Generation

In this section, given the structures from chapter 3, method for designing the control gains for

each corresponding channel from chapter 3 is introduced. Control gain generation process will be divided into three sections: Longitudinal conventional section, longitudinal TBAC section, and lateral section.

## 4.1 Longitudinal Gain Generation

### *4.1.1 Pitch Channel Gains*

The blue triangle boxes in figure 1 indicate the control gains of the autopilot, which should be a reasonable value to obtain satisfied control output. To relieve the efforts of the designer, the automated gain generation technique is applied. Pitch angle controller, which is the inner loop of the altitude controller, is designed by following procedure, for example. First, the plant is defined as follows.

$$\frac{q(s)}{\delta_e(s)} = G(s) = \frac{N(s)}{D(s)} = \frac{b_1 s + b_0}{s^2 + a_1 s + a_0} \quad (7)$$

$$\frac{\theta(s)}{\delta_e(s)} = \frac{1}{s} G(s) = \frac{N(s)}{sD(s)} \quad (8)$$

Equations (7) and (8) indicate the transfer functions of the linear dynamics. The transfer function $\theta / \theta_{cmd}$ could be obtained by closing a loop around the $q$ loop as figure 1 suggests. The transfer function $\theta / \theta_{cmd}$ is expressed in following equation.

$$\frac{\theta}{\theta_{cmd}} = \frac{K_\theta G(s)}{s(1 + K_q G(s)) + K_\theta G(s)} = \frac{K_\theta G(s)}{s[D(s) + K_q N(s)] + K_\theta N(s)} \quad (9)$$

By plugging (7) into (9), it yields

$$\frac{\theta}{\theta_{cmd}} = \frac{K_\theta (b_1 s + b_0)}{s(s^2 + a_1 s + a_0) + (sK_q + K_\theta)(b_1 s + b_0)}, \quad (10)$$

and by rearranging, it could be expressed as

$$\frac{\theta}{\theta_{cmd}} = \frac{K_\theta (b_1 s + b_0)}{s^3 + (a_1 + K_q b_1) s^2 + (a_0 + K_q b_0 + K_\theta b_1) s + K_\theta b_0}. \quad (11)$$

By observing the denominator of (11) and deriving a conventional 3rd order polynomials, it could be obtained as

$$\begin{aligned} \phi_{DES}(s) &= (s + \alpha)(s^2 + 2\zeta\omega s + \omega^2) \\ &= s^3 + (\alpha + 2\zeta\omega) s^2 + (2\alpha\zeta\omega + \omega^2) s + \alpha\omega^2 \end{aligned} \quad (12)$$

Here, $\alpha$, $\zeta$, $\omega$ indicate pole location, damping coefficient, and natural frequency of the theta loop, respectively. If one compares the denominator of (11) and equation (12), following relationships can be derived.

$$a_1 + K_q b_1 = \alpha + 2\zeta\omega \quad (13a)$$

$$a_0 + K_q b_0 + K_\theta b_1 = 2\alpha\zeta\omega + \omega^2 \quad (13b)$$

$$K_\theta b_0 = \alpha\omega^2 \quad (13c)$$

From (13a) and (13c), following expressions could be achieved.

$$K_q = \frac{\alpha + 2\zeta\omega - a_1}{b_1} \quad (14a)$$

$$K_\theta = \frac{\alpha\omega^2}{b_0} \quad (14b)$$

After obtaining the above expressions, substituting (13b) with (14a) and (14b), following expression yields.

$$\left(1 - \frac{b_1 \alpha}{b_0}\right)\omega^2 + \left(2\alpha\zeta - \frac{2\zeta b_0}{b_1}\right)\omega + \left[-a_0 - \frac{b_0}{b_1}(\alpha - a_1)\right] = 0 \quad (15)$$

Solving for $\omega$ from above equation and plugging back into (14a) and (14b) and applying reasonable user input values, $\zeta$ and $\alpha$, will provide the controller gains of $K_q$ and $K_\theta$.

### *4.1.2 Altitude Channel Gains (Conventional)*

Altitude controller design starts with the assumption that the system is a fast 2nd order system ($\omega >> \alpha$). Then, the pitch loop equation in previous section can be simplified as

$$\frac{\theta}{\theta_{cmd}} = \frac{K_p \omega^2 (b_1 s + b_0)}{(s + \alpha)(s^2 + \zeta\omega s + \omega^2)} \approx \frac{K_p (b_1 s + b_0)}{(s + \alpha)} \quad (16)$$

Here, by using the relationships of $K_p = K_\theta / \omega^2$ and $K_p b_0 = \alpha$, above equation can be derived as such.

$$G^{\theta}_{\theta_{cmd}}(s) = \frac{\theta(s)}{\theta_{cmd}(s)} = \left(\frac{b_1}{b_0} s + 1\right) \Big/ \left(\frac{1}{\alpha} s + 1\right) \quad (17)$$

Then, by applying the altitude loop gain and command filter, it yields

$$\theta_{cmd} = K_\alpha \left(\frac{k}{s + k}\right)(h_{cmd} - h) \quad (18)$$

Then, closing the altitude loop with the relationship $h(s) = (V_t / s)\theta(s)$, altitude control loop is structured as in the following figure.

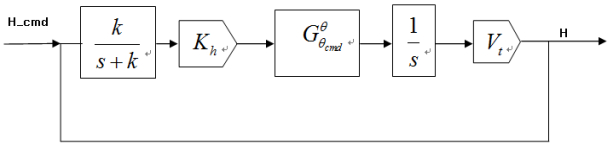


Fig. 4. Altitude Control Structure

From above structure, following transfer function is derived with several term rearrangements.

$$\frac{h(s)}{h_{cmd}(s)} = \frac{\alpha k k_h V_t \left(\frac{b_1}{b_0}s+1\right)}{s^3+(k+\alpha)s^2+\alpha\left(k+kk_hV_t\frac{b_1}{b_0}\right)s+\alpha kk_hV_t} \quad (19)$$

Similar to the approach in previous section, comparing the terms in the denominator of above equation and a conventional 3rd order equation allows the gain derivation. Conventional 3rd order polynomial in this case is expressed as

$$\phi_{des}(s) = (s+\beta)(s^2+2\zeta_1\omega_1 s+\omega_1^2) = s^3+(\beta+2\zeta_1\omega_1)s^2+(2\beta\zeta_1\omega_1+\omega_1^2)s+\beta\omega_1^2 \quad (20)$$

where $\beta$, $\omega_1$, and $\zeta_1$ are pole location, natural frequency, and damping coefficient, respectively. Applying identical process as previous section, the altitude loop gain $k_h$, and command filter gain $k$ can be obtained as follows.

$$k = \beta - \alpha + 2\zeta_1\omega_1 \quad (21a)$$

$$k_h = \frac{\beta\omega_1^2}{\alpha k V_t} = \frac{\beta\omega_1^2}{\alpha V_t(\beta-\alpha+2\zeta_1\omega_1)} \quad (21b)$$

### 4.1.3 Altitude Channel Gains (TBAC)

For TBAC altitude channel design, control structure is shown in figure 5.

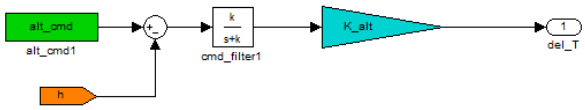


Fig. 5. Altitude Control Structure for TBAC

As the figure suggests, the control signal goes to the throttle input. To derive the altitude gain, we use the fact that an increase in throttle leads to angle of attack increase, which will finally lead to the altitude increase. Following is the state equations for angle of attack and altitude.

$$\begin{bmatrix}\dot{\alpha}\\ \dot{h}\end{bmatrix} = \begin{bmatrix}\frac{Z_\alpha}{V_t} & \frac{Z_h}{V_t}\\ -V_t & 0\end{bmatrix}\begin{bmatrix}\alpha\\ h\end{bmatrix} + \begin{bmatrix}Z_{\delta_T}\\ 0\end{bmatrix}\delta_T \quad (22)$$

Inverting above equation and calculating for $h(s)/\delta_T(s)$ will give

$$G_{\delta_T}^h(s) = \frac{h(s)}{\delta_T(s)} = \frac{-Z_{\delta_T}V_t}{s^2-\frac{Z_\alpha}{V_t}s+Z_h} \quad (23)$$

By applying the altitude gain and command filter as in figure 5, it yields

$$\frac{h(s)}{h_{cmd}(s)} = \frac{-kK_{alt}Z_{\delta_T}V_t}{s^3-\left(k-\frac{Z_\alpha}{V_t}\right)s^2+\left(Z_h-\frac{Z_\alpha}{V_t}k\right)s+Z_hk-kK_{alt}Z_{\delta_T}V_t} \quad (24)$$

Then, applying similar comparison technique as in the previous sections will give the altitude gain and the command filter gain as follows.

$$K_{alt} = \frac{\left(Z_h-\frac{\alpha\omega^2}{k}\right)}{Z_{\delta_T}V_t} \quad (25a)$$

$$k = \frac{Z_\alpha}{V_t}+\alpha+2\zeta\omega \quad (25b)$$

### 4.1.4 Velocity Channel Gains (Conventional)

Velocity is mainly controlled by throttle level in a conventional aircraft. Corresponding velocity state equation is obtained as such.

$$\dot{V}_t = X_V V_t + X_{\delta_T}\delta_T \quad (26)$$

Then, by taking the Laplace transform, it becomes

$$sV_t(s) = X_V V_t(s) + X_{\delta_T}\delta_T(s) \quad (27)$$

Then rearranging the above equation gives the following transfer function.

$$G_{\delta_T}^{V_t} = \frac{V_t(s)}{\delta_T(s)} = \frac{X_{\delta_T}}{s-X_V} \quad (28)$$

Applying the velocity gain as well as its integration gain, transfer function becomes

$$V_t = \left(K_{Vt}+\frac{K_{Vti}}{s}\right)\left(\frac{X_{\delta_T}}{s-X_V}\right)V_{tcmd} \quad (29)$$

Then, closing the loop, it yields

$$\frac{V_t}{V_{tcmd}} = \frac{X_{\delta_T}K_{Vt}s+X_{\delta_T}K_{Vti}}{s^2+(X_{\delta_T}K_{Vt}-X_V)s+X_{\delta_T}K_{Vti}} \quad (30)$$

Conventional second order polynomial is given as

$$\phi_{des}(s) = s^2+2\zeta\omega s+\omega^2 \quad (31)$$

Applying the comparison technique as in previous sections, the gains for the velocity loop gain as well as its integral gain are derived as follows.

$$K_{Vti} = \frac{\omega^2}{X_{\delta_T}} \quad (32a)$$

$$K_{Vt} = \frac{2\zeta\omega+X_V}{X_{\delta_T}} \quad (32b)$$

### 4.1.5 Velocity Channel Gains (TBAC)

In TBAC, since the velocity is controlled by the change in pitch angle, design process starts with following assumption. First, when the pitch

angle $\theta$ is increased by $\delta\theta$, then the thrust $\delta_T$ is decreased by $mg\delta\theta$ due to the gravitational effect, and vice versa. Such condition is expressed in the following equation.

$$\theta + \delta\theta \approx \delta_T - mg\delta\theta \tag{33}$$

Then, the following relationship can be obtained from equation (33).

$$\delta_T = \theta + \delta\theta(1+mg) \tag{34}$$

The transfer function from throttle to the velocity is defined as follows.

$$G_{\delta_T}^{V_t} = V_t(s)/\delta_T(s) \tag{35}$$

Substituting equation (34) into equation (35) gives

$$G_{\delta_T}^{V_t} = \frac{V_t}{\theta + \delta\theta(1+mg)} \tag{36}$$

Solving above equation for the velocity gives

$$V_t = G_{\delta_T}^{V_t}[\theta + \delta\theta(1+mg)] \tag{37}$$

Then, dividing both sides by the pitch angle, the following equation could be obtained.

$$\frac{V_t}{\theta} = \frac{G_{\delta_T}^{V_t}[\theta + \delta\theta(1+mg)]}{\theta} \tag{38}$$

Adding the assumptions $\delta\theta \approx \theta$ and $mg >> 2$ will lead to the final transfer function from the pitch angle to the velocity.

$$G_{\theta}^{V_t} = \frac{V_t(s)}{\theta(s)} = \frac{X_{\delta_T}}{s - X_V} mg \tag{39}$$

Figure 6 is the velocity control loop in TBAC system.

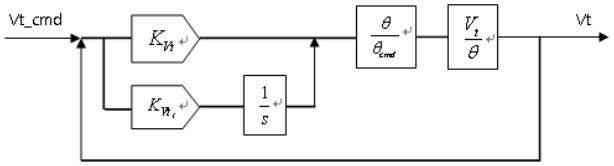


Fig. 6. Velocity Control Structure for TBAC

Figure 6 is the velocity control loop in TBAC system. Using the transfer function result from $\theta / \theta_{cmd}$ and the transfer function obtained from equation (39) will lead to the following equation.

$$\frac{\left(K_{Vt}s + K_{Vt_i}\right) X_{\delta_T} mg \left(\frac{\alpha b_1}{b_0}s + \alpha\right)}{s(s - X_v)(s + \alpha)} \tag{40}$$

By closing the loop and rearranging will yield

$$\frac{V_t(s)}{V_{t_{cmd}}(s)} = \frac{mgX_{\delta_T}K_{V_t}\alpha\frac{b_1}{b_0}s^2 + mgX_{\delta_T}(K_{V_{ti}}\alpha\frac{b_1}{b_0} + \alpha K_{V_t})s + K_{V_{ti}}\alpha mgX_{\delta_T}}{s^3 + [(\alpha - X_v) + mgX_{\delta_T}\alpha\frac{b_1}{b_0}K_{V_t}]s^2 + [mgX_{\delta_T}(K_{V_{ti}}\alpha\frac{b_1}{b_0} + \alpha K_{V_t}) - X_v\alpha]s + K_{V_{ti}}\alpha mgX_{\delta_T}} \tag{41}$$

Also, applying the same technique, derived gains are

$$K_{V_t} = \frac{\gamma + 2\zeta\omega + X_V - \alpha}{mgX_{\delta_T}\alpha(b_1/b_0)} \tag{42a}$$

$$K_{V_{ti}} = \frac{\gamma\omega^2}{\alpha mgX_{\delta_T}} \tag{42b}$$

where $\gamma$ is the pole location, and $\zeta$ is damping.

## 4.2 Lateral Gain Generation

Lateral control gains can be obtained with the similar process as the longitudinal control gains.

### *4.2.1 Heading Autopilot Gains*

In order to obtain the heading autopilot and roll SCAS gains, the process begins with the roll angle controller design. Transfer function from aileron to the roll rate is obtained as

$$G_{\delta_a}^{p} = \frac{p(s)}{\delta_a(s)} = \frac{L'_{\delta_a}}{s - L'_p} \tag{43}$$

Closing the loop and applying the roll rate gain results

$$\frac{p}{p_{cmd}} = \frac{L'_{\delta_a}}{s - L'_p + K_p L'_{\delta_a}} \tag{44}$$

As it is suggested in figure 3, roll rate loop is the inner loop of the roll angle loop. Then, resulting closed loop transfer function (after gains are applied) from roll command to the roll angle output is

$$\frac{\phi}{\phi_{cmd}} = \frac{K_\phi L'_{\delta_a}}{s^2 + (K_p L'_{\delta_a} - L'_p)s + K_\phi L'_{\delta_a}} \tag{45}$$

Finally, the roll angle is surrounded by the heading loop with several applied gains, and this relationship can be expressed as the following equation, which indicates the final transfer function of the heading loop.

$$\frac{\psi}{\psi_{cmd}} = \frac{K_\psi K_\phi L'_{\delta_a}(g/V_T)}{s^3 + (K_p L'_{\delta_a} - L'_p)s^2 + K_\phi L'_{\delta_a} s + K_\psi K_\phi L'_{\delta_a}(g/V_T)} \tag{46}$$

By comparing the denominator terms with corresponding 3rd order polynomial terms will lead to the following gain equations.

$$K_p = \frac{\alpha + 2\zeta\omega + L'_p}{L'_{\delta_a}} \tag{47a}$$

$$K_\phi = \frac{2\zeta\omega\alpha + \omega^2}{L'_{\delta_a}} \tag{47b}$$

$$K_\psi = \frac{V_T\alpha\omega}{g(2\zeta\alpha + \omega)} \tag{47c}$$

where $\alpha$ is the pole location, and $\zeta$ is damping.

### 4.2.2 Yaw Damper Gains

Yaw damper gain design process starts with the transfer function from rudder to yaw rate.

$$G_{\delta_r}^{r} = \frac{r(s)}{\delta_r(s)} = \frac{N'_{\delta_r}}{s - N'_r} \tag{48}$$

Applying the yaw damper gain $K_r$ and the washout filter $(s/(s+\alpha))$, and closing the loop yields

$$\frac{r}{r_{cmd}} = \frac{G_{\delta_r}^{r}}{1 + \frac{N'_{\delta_r}}{s - N'_r} K_r (\frac{s}{s+\alpha})} = \frac{N'_{\delta_r}(s+\alpha)}{s^2 + (K_r N'_{\delta_r} + \alpha - N'_r)s - N'_r\alpha} \tag{49}$$

Comparing the denominator terms with 2nd order polynomial gives the following yaw damper gain.

$$K_r = \frac{2\zeta\omega + N'_r - \alpha}{N'_{\delta_r}} \tag{50}$$

### 4.2.3 ARI Gain

Aileron-Rudder Interconnection (ARI) gain can be obtained by using transfer functions from aileron and rudder to sideslip angle, and they are listed in the following equations.

$$G_{\delta_A}^{\beta} = \frac{N'_{\delta_a}}{s - (Y_\beta / V_t)} \tag{51a}$$

$$G_{\delta_r}^{\beta} = \frac{N'_{\delta_r}}{s - (Y_\beta / V_t)} \tag{51b}$$

ARI gain can be expressed as the negative ratio of transfer functions of aileron to sideslip angle to rudder to sideslip angle, and it is shown in (52).

$$K_{ARI} = -\frac{G_{\delta_A}^{\beta}}{G_{\delta_r}^{\beta}} = -\frac{N'_{\delta_a}}{N'_{\delta_r}} \tag{52}$$

An important assumption should be considered in this case, which is the actuator dynamics of aileron and rudder should be identical.

## 5 Linear Analysis

With the gains generated from the previous section, time domain responses from each channel and frequency domain linear analysis based on Mil-F-8785C are to be applied in order to provide the credibility of the designed controller. In Mil-F-8785C the levels of flying quality are considered as the main criteria of aircraft performance assessment [7]. The levels of flying qualities defined by Mil-F-8785C are as follows [2,7].

***Level 1.*** *Adequate for the mission flight phase.*

***Level 2.*** *Some increase in pilot workload or degradation in mission effectiveness exists.*

***Level 3.*** *Pilot workload is excessive, or mission effectiveness is inadequate, or both.*

By the flying quality criteria, level 1 indicates the ideal condition for a perfect flight. Therefore, the aircraft controller designed with the algorithms from section 4 should satisfy level 1 conditions for all dynamic modes of the aircraft. Graphs in this section indicate under what flying quality level the designed controller's dynamic performance would fall. The flight phase is 'category B' since the controller is designed for the cases of climb, cruise, and descend. The aircraft classification is class I, which is for small and light weight aircrafts.

Figures 7 to 11 indicate the flying qualities from short period damping, phugoid damping, short period frequency, Dutch roll damping and frequency, roll mode, and spiral mode. Red dots indicate what level the current performances fit in. Figures also indicate that in all criteria, the controller gives outstanding performances in every flying quality criteria by satisfying level 1. Satisfying level 1 means that the designed controller is eligible for carrying out the missions.

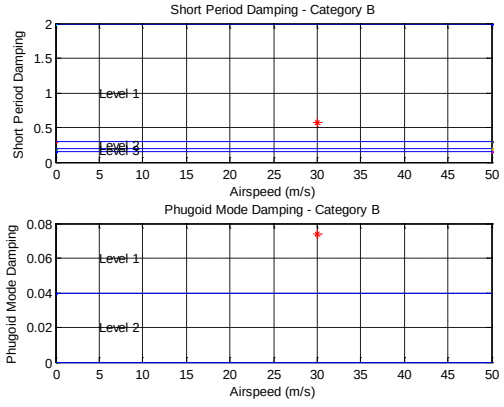


Fig.7. Short period and Phugoid mode Damping

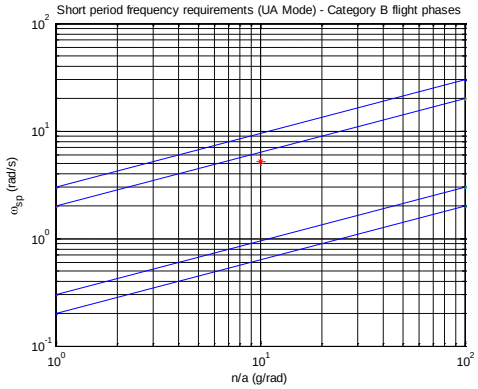


Fig. 8. Short Period Frequency Requirements

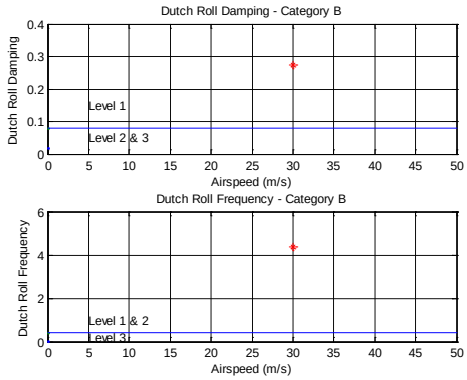


Fig. 9. Dutch Roll Damping and Frequency

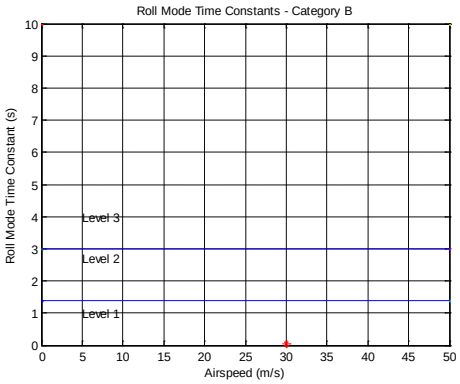


Fig. 10. Roll Mode Time Constant

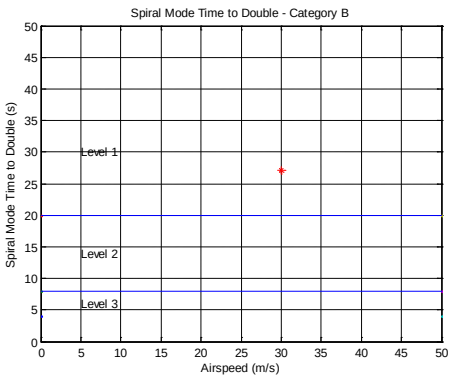


Fig. 11. Spiral mode Time to Double

## 6 Simulation Results

In this section, several simulations are conducted to observe the convergence behaviors of the aircraft. Simulations are performed in longitudinal, lateral, and combined three dimensional situations. Table 1 shows the physical data of the UAV used for the simulation.

Table 1. Physical Data of the UAV

| Mass | Wing Area | Wing Span | MAC |
|---|---|---|---|
| 53 kg | 1.682 $m^2$ | 3.912 m | 0.465 m |

All simulations begin from the initial conditions of 35 m/s velocity, 100 meter altitude, and 0 heading angle.

### 6.1 Longitudinal Channel Simulation

Figure 12 shows the velocity and altitude responses with the given control commands of 40 m/s velocity and the altitude of 140 meters. Figure 13 shows the corresponding control surface input responses of thrust and elevator.

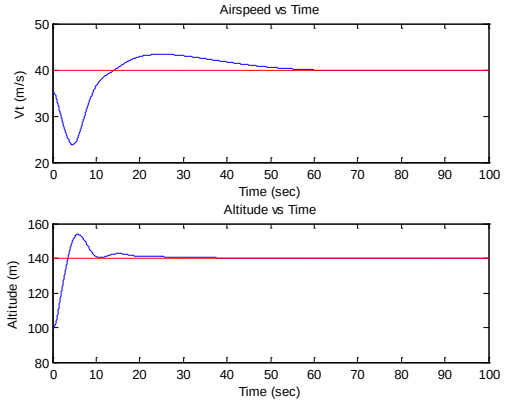


Fig.12. Velocity and Altitude Responses

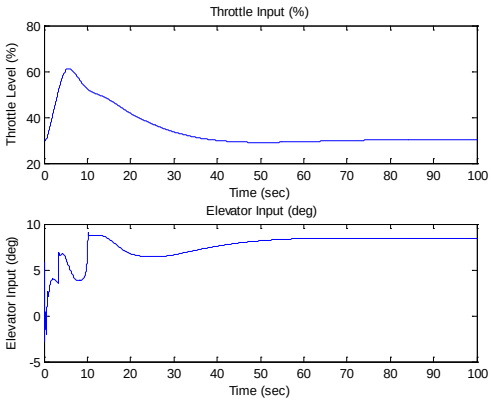


Fig.13. Thrust and Elevator Responses

As the responses indicate, with some overshoot in the altitude channel, the aircraft's velocity and altitude properly converges to its command values. It is noticeable that the velocity converges a bit slowly, and it is due to the slow dynamics of the engine. Figures 14 and 15 give the results for TBAC mode. Altitude hold simulation for this mode is well performed by observing the response. Notice that the altitude command convergence is slower than that of the conventional type due to its slow dynamics from the throttle level of the engine. Figure 15 shows that throttle level increases to gain the altitude of 50 meters, and elevator deflects to maintain the airspeed of 35 m/s.

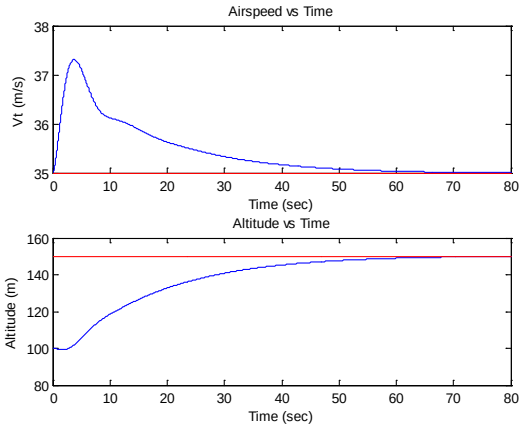


Fig.14. Velocity and Altitude Responses (TBAC)

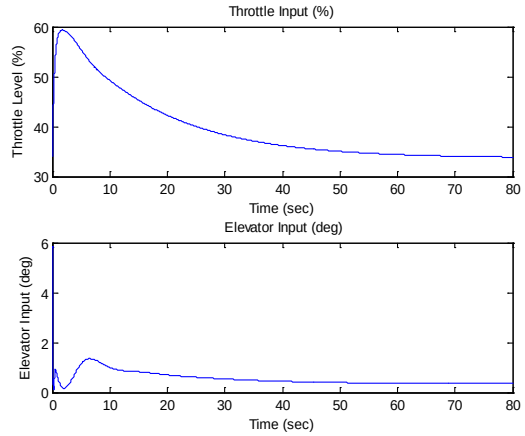


Fig.15. Thrust and Elevator Responses (TBAC)

## 6.2 Lateral Channel Simulation

For lateral channel simulation, heading hold autopilot simulation has been conducted. Heading command of 80 degrees is applied as shown in figure 16. As soon as the command is given, aircraft performs a banked turn to follow the command. After the heading angle converges to its command, bank angle of the aircraft returns to its original value, zero. Figure 17 describes the aileron and rudder responses during the simulation.

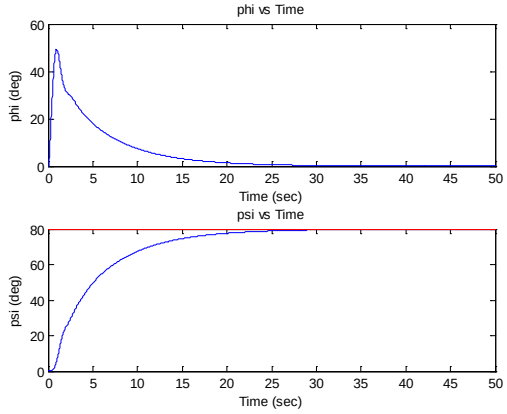


Fig. 16. Roll and Heading Angle Responses

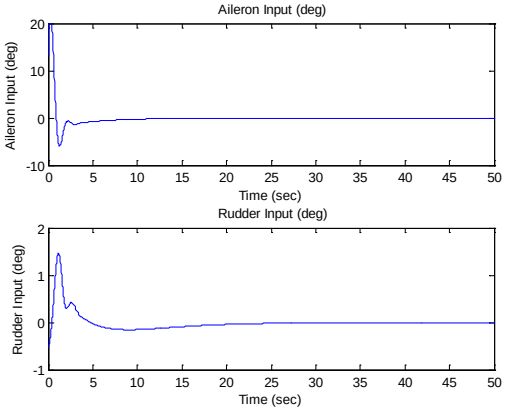


Fig. 17. Aileron and Rudder Responses

## 6.3 Three Dimensional Waypoint Guidance

In order to test whether the aircraft performs well in three-dimensional world, a simple waypoint guidance logic has been implemented to the simulation tool. In each case, the plane is tested whether it can approach to the given waypoint (blue) departing from the initial position (green). There are two waypoint guidance simulation cases, which in each case the aircraft is given with north, east, and altitude commands.

Figures 18 and 19 describe the waypoint guidance simulations with the paths of the UAV shown in red lines.

Case 1. $N_{cmd}$ = 1300$m$ $E_{cmd}$ = 800 $m$ $H_{cmd}$ = 160 $m$

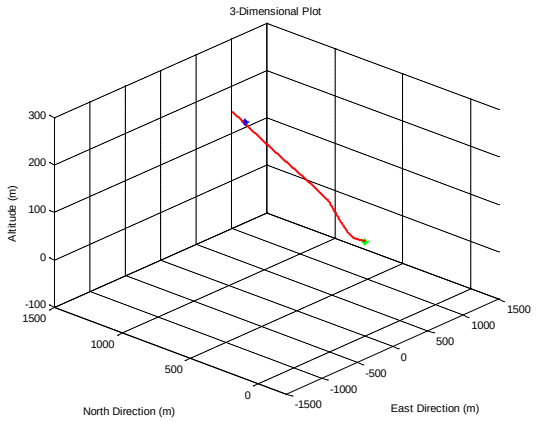


Fig. 18. Waypoint Guidance (Case 1)

Case 2. $N_{cmd}$ = 600$m$ $E_{cmd}$ = -1300 $m$ $H_{cmd}$ = 60 $m$

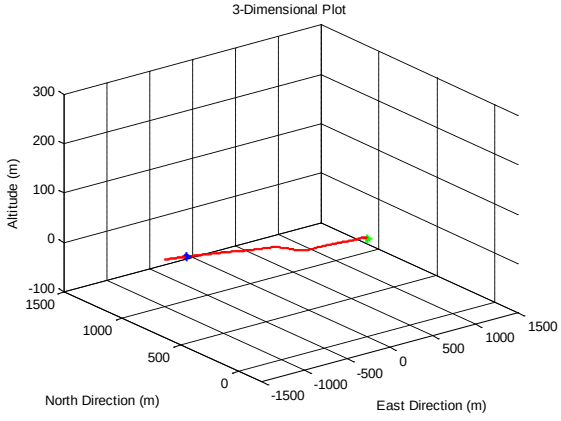


Fig. 19. Waypoint Guidance (Case 2)

In both cases, the aircraft trajectories suggest that the UAV successfully finds and arrives at the designated waypoint. It indicates that the aircraft controller is well designed and finally ready for the real-world flight tests.

## 7 Conclusion

This research suggests that the process for the controller design of an aircraft can be automated with the two inputs (pole location, damping) from each channel. All designed controller is to be applied to the gain scheduling process: the process for obtaining all possible gain sets within the aircraft's flight envelope. Linear analysis process, with the aid of Mil-F-8785C requirements, is conducted as the verification process for the designed controller. Simulation results indicate that the UAV designed with the automated design logic shows satisfactory performances in several flight simulations. In the future, the automated control design logic will be applied to real UAVs to guarantee its performance in real-world environments.

## Acknowledgement

Authors gratefully acknowledge the financial support by the Ministry of Knowledge Economy of Korea under the project of World Best Software (WBS). This research was also supported by Brain Korea 21 Project at KAIST and the project of Global Ph.D. Fellowship, which National Research Foundation of Korea conducts from 2011.

## References

[1] Davis, W., Kosicki, B., Boroson, D, Kostishack, D., "Micro Air Vehicles for Optical Surveillance," The Lincoln Laboratory Journal, Vol.9, No.2, 1996, pp.197-214

[2] Stevens, B., Lewis, F., *Aircraft Control and Simulation*, 2nd Edition: John Wiley & Sons, Inc., 2003.

[3] Kim, B., Kim, Y., Bang, H., Tahk, M., Hong, S., *Flight Dynamics and Control*, 1st Edition: Kyungmoonsa, 2007.

[4] Etkin, B., *Dynamics of Flight Stability and Control*, 3rd edition: John Wiley & Sons, 1996.

[5] Blakelock, J. H., *Automatic Control of Aircraft and Missiles*, 2nd edition: John Wiley & Sons, 1991.

[6] Yoo, D., Tahk, M., Yang, H., Choi, S., Kim, J., "A Study on Throttle based Altitude Controller Design for Unmanned Aerial Vehicles," KSAS Spring Conference, April 2012.

[7] Anon., "Military Specification, Flying Qualities of Piloted Airplanes," Department of Defence, MIL-F-8785C, Washington, D.C., November 1980.

## Copyright Statement